Chapter 6
The Role of Photon Statistics in Visual Perception

Leonid Krivitsky and Vadim Volkov

Abstract We address the question of how fundamental photon fluctuations are perceived by a live visual system. The discussion is focused on specific type of photoreceptor cells within the eye, known as retinal rod cells. Rod cells provide vision under low light conditions and they are sensitive at a single photon level. We review experiments on interaction of the rod cells with light sources of different photon statistics, including coherent, pseudo-thermal, and single-photon sources. Accurate control over photon statistics of light stimuli, combined with technique for the readout of rod cells response, enable precise and unambiguous characterization of intrinsic features of the visual system at single and discrete photon levels.

6.1 Retinal Rod Cells

The eye represents a unique device for visual perception that developed over millions of years of evolution. Its mode of operation is perfectly tuned and well organized. In fact, some of the features of modern optical engineering can be readily found in live visual systems. Examples include broad-band polarization retardation plates in the eyes of crustacean, polarization sensitive vision of desert ants that helps to navigate under a clear sky, gradient index lenses found in compound eyes of insects that minimize aberrations, and many others.

L. Krivitsky (✉)
Institute of Materials Research and Engineering, Agency for Science Technology and Research (A*STAR), Singapore, Singapore
e-mail: Leonid_KRIVITSKIY@imre.a-star.edu.sg

V. Volkov
Faculty of Life Sciences and Computing, London Metropolitan University, London, UK
e-mail: vadim.s.volkov@gmail.com

V. Volkov
Department of Plant Sciences, University of California, Davis, CA, USA

R. W. Boyd et al. (eds.), *Quantum Photonics: Pioneering Advances and Emerging Applications*, Springer Series in Optical Sciences 217,
https://doi.org/10.1007/978-3-319-98402-5_6

Specialized cells within the eye, known as retinal photoreceptors, are responsible for sensing light by converting it into the form of electrical pulses. In vertebrates photoreceptors are arranged in a layer, which forms a part of multi-layered retina tissue at the back of the eye. The retina amplifies visual signals and transfers them to neurons of the optic nerve for further processing by the brain. There are two types of photoreceptor cells: cone cells are responsible for colour vision in day light conditions and more sensitive rod cells provide uncoloured vision under low light conditions [1].

The present study is inspired by the ultimate sensitivity of retinal rod cells down to the single photon level. This remarkable property makes them a perfectly suited system for fundamental studies of the role of quantum effects in photochemistry, neurobiology and perception. From the technological standpoint it is highly intriguing that a single rod cell of an average length of about 50 μm and diameter about 5 μm represents a self-contained single photon detector, which includes a light sensitive pigment, an ATP power supply, and a synaptic terminal that links it to the rest of retina. Such a compact arrangement surpasses modern man-made devices which are more bulky and often have technological limitations. Further insights into functions of rod photoreceptors could define the properties required for a new family of sensitive light sensors, mimicking natural detection.

6.1.1 Morphology of Rod Cells

Vertebrate retinal rod photoreceptor cells have a typical rocket like shape, see Fig. 6.1. They consist of two distinctive morphological functional regions: extended rod-like outer segment (ROS) which is filled with photopigment molecules represented by rhodopsin, and shorter rounded inner segment (RIS) which contains components of cell machinery.

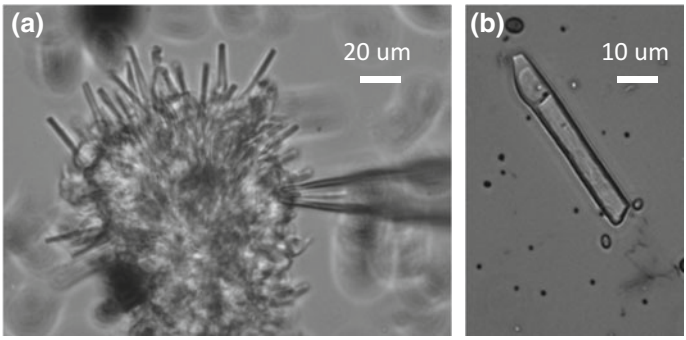

Fig. 6.1 Microscope image of isolated *Xenopus laevis* retinal cells (**a**) and a rod cell from the preparation (**b**). Adapted from [105]

Typical size of rod cells is about 2–10 μm in diameter and about 15–100 μm long, the values depend on taxonomic group of animals. Rods of mammals are smaller in diameter than amphibian ones, about 2 μm compared to 5–8 μm, correspondingly. The diameter of rods in retina of birds is also about 2 μm (e.g. for owls [2]), close to the estimated theoretical limit (based on morphometric analysis) for the diameter of rod cells to be 1.2 μm [3]. Still the typical diameters of rods of e.g. African frog *Xenopus* are about 10 wavelengths of red light. Technically speaking, the theoretical resolution of human retina with rods being about 2 μm in diameter is 12,550 dots per inch. The value is comparable to state-of-art charge-coupled device (CCD) cameras, and is sufficient to resolve the tiny details of the surrounding world. Likely, that the high resolution of the retina is naturally restricted by the wavelength of the visible light.

6.1.2 Light Detection by Rod Cells

The basis for light detection by the rod cells is as follows. Rod cells contain large number of pigment molecules in their outer segment. For example, mouse rod contains nearly hundred millions of rhodopsin molecules (reviewed in [4]). A pigment molecule absorbs photon and changes its conformation; the change is amplified by molecular networks of the corresponding rod cell and may result in physiological responses.

More details require knowledge about the structure of rod cells and molecular and physiological mechanisms of signal amplification and transduction in visual receptors. Oblong rod cells have numerous stacked disks at the ROS; the disks are formed by membranes with a rhodopsin photo-pigment [1]. Large number of disks, e.g., about 800 for a mouse rod [4] or about 1500–2000 for an amphibian rod cell [5], multiplied by huge number of rhodopsin molecules per the disk, about $8 * 10^4$ per a disk in the mouse rod, results in nearly hundred millions of rhodopsin molecules per a typical mouse rod [4] or more, about $3 * 10^9$, per an amphibian rod cell [5]. A molecule of rhodopsin consisting of retinal and protein part opsin absorbs photon, changes conformation and isomerizes to metarhodopsin.

Metarhodopsin has a short life half-time, hence special precautions were taken to crystallize this G-protein coupled receptor and solve its structure [6] adding to the earlier crystal structure of rhodopsin [7] and understanding the transformation of rhodopsin after absorption of a photon.

Amplification of a signal from activated rhodopsin occurs via further activation of G-protein transducin, see Fig. 6.2. Transducin is composed of α, β and γ subunits, it laterally diffuses on the surface of disk membrane and interacts with metarhodopsin. The result of the interaction is that transducin changes bound GDP for GTP (reviewed in [8–10]). Activated α-subunit-GTP of transducin binds phosphodiesterase (PDE) with stoichiometry 2 to 1, thus activating PDE. PDE is

enzyme which hydrolyses cyclic nucleotide cGMP to nucleotide GMP, hence concentration of free cGMP in cytoplasm of a rod cell and more in ROS decreases nearly two times from about 2–4 μM [11–13]. The drop in cGMP closes cyclic nucleotide gated ion channels (CNGCs) of rod cell membrane, because the ion channels are regulated (gated) by bound cGMP [14, 15]. The channels are in an open state in darkness under higher μM concentration of cGMP. Lowered cGMP under illumination closes them in a strong concentration-dependent manner due to four cooperative sites of cGMP binding for the functional channel molecules (reviewed in: [13, 16]). Rod cell membrane hyperpolarizes with closed CNGCs. Finally the initial absorption of a photon results in the decrease of membrane potential to more negative values and gives rise to corresponding ion current, the hyperpolarisation is further passed to neurons of visual nerves (reviewed in: [8–10]).

In reality the basic scheme of physico-chemical events from photon absorption by rhodopsin to membrane depolarisation in rod cell due to closure of CNGCs is much more complicated. It includes numerous feedbacks, mechanisms of regulation, signal/noise suppression and stable and robust amplification of signal. Without excessive over complication we can calculate basic parameters corresponding to absorption of one photon, see Fig. 6.3. The quantum yield of rhodopsin transformation was estimated over 0.6 (reviewed in [17]), then one molecule of metarhodopsin R* can activate up to hundreds of transducin (G* for active form) molecules [8, 18]. Rate of activation is around 125 $G^* s^{-1}$ per R* for amphibian rods at room temperature and about 3 times higher in mammalian rods at body temperature [10]. Transducin activates PDE (ratio 1:500 was proposed for R* to activated PDE [18]) and finally up to 10^5 cGMP molecules are hydrolyzed per photolyzed rhodopsin [5]. Further estimates include volume V for a typical retinal rod cell (cylinder with diameter about 5 μm and length about 50 μm) of *Xenopus* toad being about 1000 $\mu m^3 = 1$ pL $= 10^{-15}$ m^3 and surface area S around 1600 μm^2. Hence, about 10^5 cGMP molecules are equal to concentration of about $10^5/(V * N_a) = 10^{17}/(6.02 * 10^{23}) \approx 0.16$ μM, where N_a is Avogadro constant. The real changes in the concentration of cGMP after absorption of a single photon are to be higher and located within a much smaller volume of the ROS.

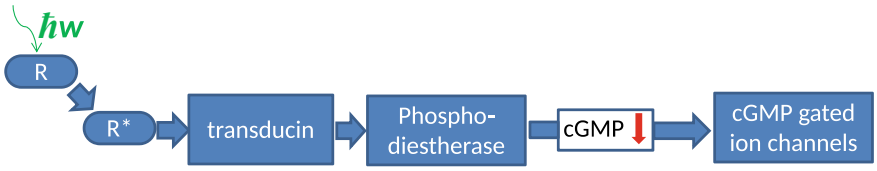

Fig. 6.2 Signal transduction chain in a vertebrate retinal rod cell starting from a photon hν and leading to cyclic nucleotide gated channels. Closure of the ion channels after drop in cGMP results in membrane hyperpolarisation and stops inward ion current of sodium and calcium. Adapted from [105]

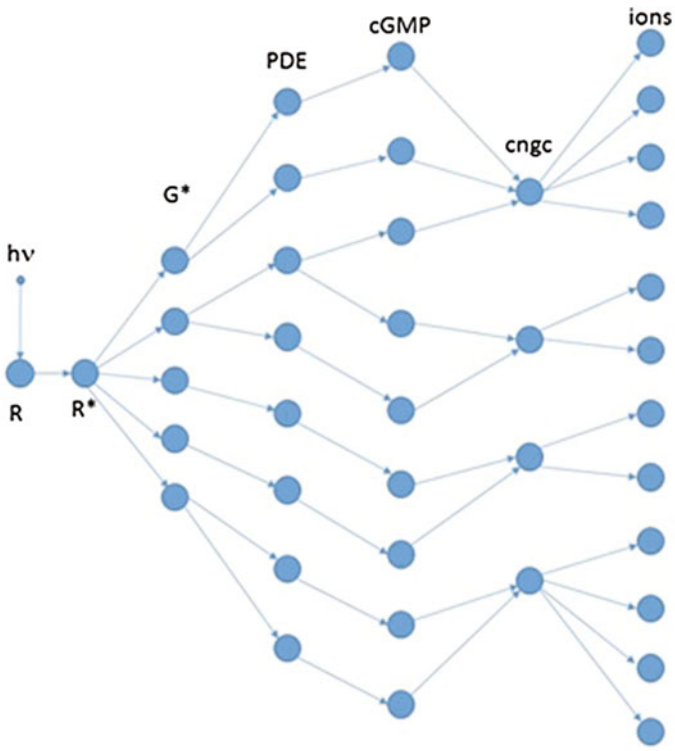

Fig. 6.3 Directed graph of interacting elements for modelling signal transduction in a vertebrate rod cell after influence of one absorbed photon. R is rhodopsin, R* is activated rhodopsin, which activates over 100 transducin G* molecules and in turn about 500 phosphodiesterase PDE molecules. PDE reduces concentration of cGMP for about 10^5 molecules/R* or about twice from 2 μM, drop in cGMP closes cGMP-gated ion channels (CNGCs); it changes membrane potential and ion fluxes via membrane. The number of affected molecules is indicative and was determined in multiphoton experiments, where changes depend on duration and intensity of light stimulus. Not all the components are included for initial simplicity (e.g., Ca^{2+} signalling, lipid signalling etc.), while further interactions in prolonged multiphoton experiments may include alteration in gene expression and physiological state of the rod cells. Not all the interactions are confirmed for single photon experiments

6.1.3 Mechanisms of Reproducibility for Light-Induced Responses of Rod Cells

The molecular machinery for detection of photons by rod cells (1) should provide that the electric response is proportional to the number of absorbed photons, (2) has to ensure feedbacks to quench the activated rhodopsin (metarhodopsin R*) and (3) needs to terminate the signal amplification. Without these mechanisms a single photon would trigger a chain reaction in the cell and the light signal would be distorted, thus providing false information about the real world.

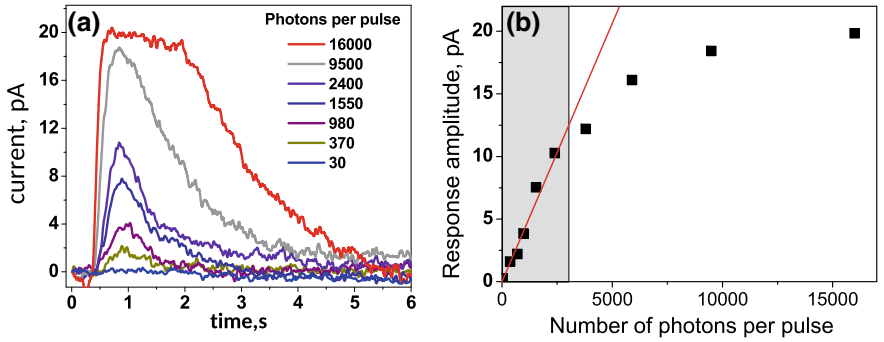

Fig. 6.4 **a** Kinetics of retinal rod responses of *Xenopus laevis* to pulses of light. The colour legend indicates the corresponding number of impinging photons, which were emitted from the tip of the optical fiber (number of photons is not adjusted for the efficiency of light delivery to the cell). **b** The corresponding dependence of the amplitude of the cell response on the number of impinging photons. The grey shaded area shows the region of the linear response. From Sim et al. [99]. Results for this figure and for Figs. 6.5, 6.6, 6.7, 6.8, 6.9, 6.10, 6.11 and 6.12 are for the rod cells from dark adapted retinas of frogs *Xenopus laevis*

Increase of the number of photons impinging on a rod cell increases the electric current recorded from the cell in a reproducible manner, Fig. 6.4a, b. The higher number of photons activates more rhodopsin molecules, hence the response amplitude is higher; the response amplitude reached saturation at around 25–30 absorbed photons per light pulse for *Xenopus* rod cells [19].

Molecular networks for termination of signal in rods include many proteins and protein macromolecular complexes. Under dark conditions metarhodopsin, activated transducin and PDE are deactivated, then concentration of cGMP returns to earlier higher values resulting in depolarization of the membrane. These processes determine temporal and kinetic components of the light-induced events in rods (reviewed in [20]). Inactivation involves several fast steps: for example, in mouse rods the activity of R* is quenched with half-time about 50–80 ms [21, 22] by successive phosphorylation by rhodopsin kinase and further binding of the protein arrestin [20]. Each of the proteins, rhodopsin kinase and arrestin, in turn has their own regulation feedbacks and loops.

The kinetics of light-induced photocurrent in rods, shown in Fig. 6.4, can be reasonably well described by several mathematical models, which account for kinetics of individual photon-induced reactions, kinetics of inactivation, and the morphology of rod cells [20, 23, 24]. It is worth to mention that reproducibility of electric output from a rod cell after absorption of a single photon is remarkably stable. At a first glance it seems that the numerous stochastic probabilistic components would make the response also stochastic with high variability. However, the numerous feedbacks, cooperativity of interactions and buffering of concentrations by diffusion rates make the responses relatively robust [20]. Inactivation components are especially important for ensuring the reproducibility [24, 25]. Modelling was performed using detailed geometry to imitate rod disks as circles

with known incisures [24]. Results led to conclusions that diffusion rates of cGMP and the other second messenger and regulator Ca^{2+} in cytoplasm are the main suppressors of variability which occurs in the activation cascades [24]. Concentration of Ca^{2+} ions is one more regulator of cGMP-gated ion channels (reviewed in: [26]). Charged amino acid glutamate residue is located in the pore of the protein which forms the channels; this amino acid residue is responsible for block of the inward current through ion channels by micromolar Ca^{2+} concentrations [27]. Ca^{2+} ions are also passing via the channels and add an additional feedback regulation loop.

An important role in optimization of the signal-to-noise ratio in rod cells is played by cooperativity of interactions and by low electric conductance of cGMP-gated ion channels. The natural choice was to select a large number of ion channels with abnormally low conductance, hence thermal fluctuations of gating for a single ion channel will be averaged and have no significant effect on the membrane potential. About 500 cGMP-gated ion channels are estimated per μm^2 in salamander rods making the total number around $5 * 10^5$ per the cell with a small fraction of 1–2% being open even in darkness (reviewed in: [28]). A single channel has tiny conductance of 100 fS or approximately 3 fA at −30 mV in a standard Ringer medium [14]; (reviewed in: [28]). Several hundreds and thousands of channels are required for response to one photon and multiphoton pulse, respectively. It allows the passage of about $2 * 10^4$ monovalent cations per second per a single channel at −30 mV. One more, but slower component of noise originates from transduction cascade due to spontaneous thermal activation of PDE and the other component originates from thermal activation of rhodopsin with low probability of 10^{-10} (reviewed in: [29]).

Our present knowledge and recent progress in molecular biology already offer opportunities to manipulate the light-induced electric responses of a rod cell. There are numerous mutations influencing components of the signal transduction chain; some mutants have altered kinetics and amplitude of photocurrent (reviewed in [20]). For example, C-terminus of rhodopsin molecule has six sites for phosphorylation, they are important for inactivation of R*. Decreasing the number of the sites in mouse mutants by means of molecular biology increased the duration of photocurrent and also changed its shape [30]. It is interesting to mention that phosphorylation at amino acid residues of serine or threonine had distinct effects on photocurrent curves [31]. Earlier observations on the role of Ca^{2+} ions in phototransduction networks led to the opportunity of shaping the photocurrent by buffering Ca^{2+} in cytoplasm of rod cells. Ca^{2+}-chelator BAPTA kept stable Ca^{2+} concentration; it slowed Na^+/Ca^{2+} exchange current via transporters of rod cell and hence increased amplitude and duration of the total photon-induced photocurrent [32]. Less directed option of using specific inhibitors or stimulators of cell biochemistry was realised in the experiments at the beginning of 1980s. Surprisingly, inhibitors of PDE increased the electric photoresponse of rod cells though the opposite is expected according to our present knowledge [33]. The voltage change of several mV was recorded by intracellular electrodes in rod cells after light pulses. PDE inhibitors including caffeine, papaverine and several others enhanced two to

six times the voltage photoresponses [33]. Potentially these effects are linked to Ca^{2+} concentrations and need analysis from the point of systems biology. Even simpler option of changing extracellular K^+ or Cl^- concentrations has an effect on voltage decrease in rods after pulses of light [34].

6.1.4 Comparison of Photoreceptors from Different Organisms and Man-Made Photodetectors

One important note is that different biological organisms possess slightly different phototransduction chains and often quite large variation in parameters of light-induced electric responses. For example, human rod cells operate at stable body temperature, smaller in size than amphibian rods, but have shorter time to peak of the photoresponse with about 100-fold higher calculated amplification coefficient (reviewed with more comparisons in: [35]). The operating temperature and morphology could be an explanation for the phenomenon [36]. Comparative studies of retinal rods of many vertebrates revealed significant variation in amplitude of single-photon responses from 0.4 pA with signal/noise ratio (SNR) around 1.5 (amplitude over standard deviation of the biological component of dark noise) in river lamprey to 0.4–1.1 pA with SNR 1.6–3.7 in mouse according to different experimental data (reviewed in [37]). The higher SNR about 4.5 for the photoresponses was reported for rods of monkey *Macaca fascicularis* due to low background noise of rods [36].

More comparisons lead to invertebrates. Insects have no retina and rod cells, but compound eyes with light perceiving cells called ommatidia. Surprisingly, insects have similar to vertebrates phototransduction chains and architecture of retinal neurons [38], though with slightly different sequence of events for phototransduction. Fruitfly *Drosophila* is a well-known biological insect model with numerous mutants available for understanding the light perception in the ommatidia of the organism. The known differences between a fruitfly and vertebrates in phototransduction is that (1) phospholipase C is present in photoreceptors of *Drosophila* instead of PDE in vertebrates, (2) signalling via inositol trisphosphate and diacylglycerol and probably polyunsaturated fatty acids in fruitfly substitutes cGMP signalling in vertebrate rod cells, (3) phototransduction in photoreceptors of the insect results in opening of closed under darkness transient receptor potential ion channels, not closing of cGMP-gated ion channels in vertebrates (reviewed in: [39–41]). Kinetics of photoresponses to single photons in fruitfly is 10–100 faster than in vertebrate rods [42]. More variation may be found among species of numerous and strikingly unusual biological organisms.

The relatively low SNRs for vertebrate rod cells seem to be typical for biological systems compared to higher SNRs of man-made photo-detection devices. It's reasonable to analyse the sources of noise in rod cells and in engineered photodetectors. The main component of background high frequency noise in rod cells is

determined by flickering (opening-closing) behaviour of open cGMP-gated ion channels. Suggesting normal or binomial distribution for flickering amplitudes of the large number of ion channels [43, 44], it is conceivable that the noise is proportional to electric conductance of a single channel and the number of the channels. From one point, general assumptions propose limits for noise suppression in biological systems, otherwise negative feedbacks and the whole functioning of system are becoming extremely expensive: the minimum standard deviation decreases with the quartic root of the number of events for Poisson communication channels [45]. From the other point, noise could be important for the cell behaviour [46] and for interaction with neurons. Hence, it is likely that the background flickering noise of ion channels could not be essentially reduced. The single-photon signal at the background of the noise is resolved by the amplification cascades after activation of the rhodopsin, so the SNR is the result of two independent processes. Considering for instance a ten times lower SNR would prevent from recognising single photons by rod cells; ten times higher SNR would essentially shrink the range of multiphoton response since the maximal photocurrent is limited by interactions with neurons. Again, the design of rod photo-responses seems optimal. The slower sources of noise are generated by transduction cascade due to spontaneous thermal activation of PDE or thermal activation of rhodopsin with low probability of 10^{-10} [29, 47], the latter cannot be distinguished from single photon responses.

Man-made photodetectors differ in the photosensitive elements, from (1) alkali and group V metals or their alloys in photomultiplier tubes, (2) silicon or germanium photosensitive semiconductors in avalanche photodiode detectors to (3) silicon-based photodetectors in charge-coupled devices (CCDs) [48] and to (4) Niobium nitride nanowires for superconducting photodetectors [49]. Consequently, the quantum yield varies from 0.2 to 0.95 [48] compared to about 0.7 of rhodopsin. SNRs of man-made photodetectors at the single-photon level also differ and could be below 1 in Geiger-mode avalanche photodiodes [50, 51], while reaching over 100 at high light intensities [50]. More details are briefly summarised in Table 1 and potentially may provide ideas to improve the man made photodetectors.

6.1.5 Basics of Communication Between Neurons and Rod Cells

Change of electric potential in a rod cell is sensed by neurons in the retina and directed for further processing to specific regions of the brain. The giant "neural supercomputer" consists of: hundreds of neurons in worms lacking eyes, thousands and millions of neurons in insects with compound eyes and over 80 billions of neurons in the human brain [52–55]. The processing of visual information provided by photoreceptors (including retinal rod cells) is extremely complex and essentially

Table 1 Comparison of basic photodetection properties of rod cells with man-made engineered photodetectors

	Rod cells	Photomultiplier tubes	Avalanche photodiodes
Photosensor compound	Rhodopsin	Alkali and group V metals	Silicon, germanium-based or other semiconductors
Quantum yield/ efficiency	About 0.7	Usually 0.1–0.5, over 0.7 for GaAsP	Usually 0.2–0.4, though could be over 0.8 for silicon-based and other semiconductors
Transformation of signal	Photon changes the conformation of protein molecule	Light signal is directly converted to electric signal	Light signal directly excites the electron-hole pair
Number and properties of amplification cascades	Several steps including at least four amplification cascades with different properties: amplification of protein conformation, of hydrolysed cGMP, of cation current	Several multiplication cascades to amplify the initial electric current of electrons	Direct amplification of initial electric signal through impact ionization
Principle of interactions in amplification cascades	Several mechanisms including: (1) molecular interactions of diffusing proteins, which precisely recognise the corresponding proteins from the next amplification cascade; (2) chemical reactions; (3) binding of cGMP to protein ion channels; (4) final step is conversion to electric signal of ion fluxes	Electrons emitted from photocathode are multiplied by several dynodes via secondary emission of electrons	Impact ionization by electrons/holes in the multiplication region under strong electric field
Response time	Tens and hundreds of milliseconds to few seconds, high variability among species and Q_{10} in physiological range of temperatures	Around 1–20 ns depending on type, recovery time is below and around 100 ns	Around and below 1 ns, recovery time is below 50 ns

Based on Ref. [48] and manuals for present photomultiplier tubes and avalanche photodiodes

not known yet. Changes in electric potentials of individual rod cells are passed to neurons of adjacent layer in retina, then to the second layer of specialised neurons and finally to neurons of visual nerves (more details are reviewed in [56]). After several consecutive steps the electric pattern of altered electric activity is processed, modified and analysed by brain. The processing and modification involve correction for image abberations, uneven distribution of photoreceptors in retina and the other drawbacks of initial signals. However, the question rises if the electric signals from individual rod cells are reliably sensed by neurons and also provide required starting level of temporal and spatial resolution. Indeed, a photoresponse from a rod after absorption of a single photon could be too low or too high for retinal neurons. To the best of current knowledge natural retinal design is essentially the mostly optimal [57].

While the photoelectric response from a rod could be spread by means of electrically coupling the rod cells via special gap junctions of high resistance (reviewed in [56]), the same signal could be amplified in synaptic terminals of rod cells. The electric coupling between rods in the retina reduces temporal resolution, but increases signal to noise ratio; the gap junctions are the regulated contacts and potentially they offer a way to adapt to changing illumination.

Synapses are the other specific places of contacts between cells; synapses of nervous system are divided to chemical and electric ones. Briefly saying, chemical synapses are composed of two membranes of contacting cells and have a small gap of around 20 nm between the membranes. The specific chemical compounds are released by one membrane, pass the gap within milliseconds and interact with receptors or specialised ion channels at the other membrane known as postsynaptic one. It leads to depolarisation or hyperpolarisation of the corresponding neuron, which forms the postsynaptic membrane. The simple mechanisms links cell biology with electric responses of neurons, moreover it allows amplification of the signals. There could be many synapses between two adjacent neurons. Finally a "giant supercomputer" is formed consisting of numerous neurons with several potential discrete or gradual states of electric potential. Changes in electric potential are able to carry, record and process information. Recent progress in computer modelling helped to simulate the behaviour of about 31,000 real neurons of 207 revealed subtypes with approximately 8 million connections and 37 million synapses [58].

The change in electric potential of a rod cell after a response to single photon is reported from about 0.2 mV/R* to over 1.0 mV/R* [34] or similar values of 1 mV per a single absorbed photon [59]. The voltage changes correspond to measured ion currents about 0.3–1.5 pA/photon (reviewed in: [25, 37]). Small fluctuations of rod signals are effectively filtered in retinal bipolar cells owing to strong nonlinearity in synapses caused by specific ion channels [57, 60]. About 0.5 to 2 bipolar channels in transduction chains of synapses are opened in darkness whereas about 30 channels are open after response to one photon [60]. Thus the optimal natural design efficiently supresses the noise from rods [57]. One more interesting feature is that too strong signals above a certain threshold from rods are clipped by voltage gated calcium channels in synapses. It prevents from excessive voltages and, hence, the large dynamic range of photon fluxes is compressed within a narrow range of

voltages of about 5 mV [61]. However, ion currents in synapses are highly dependent on the external pH [62] and the synapses are very dynamic structures with numerous regulators [63]. It was proposed that the features convert the photovoltage range from rods for nonlinear processing by neural networks [64].

6.1.6 Readout of Rod Cell Response

Historically, response of photoreceptors to weak light flashes has been intensively studied since the 1930s with first experiments dating back to 1889 [65] and 1907 [66]. The main motivation of those studies was to determine the fundamental limit of light perception in nature and to understand its variation in different species. The experiments coincided with the prediction and discovery of photons at the beginning of the 20th century, quantum physics gave explanations and independently stimulated study of visual receptors. Early physiological approaches were based on so-called "frequency-of-seeing" experiments, when a dark adapted individual was asked about the perception ("can see"/"can not see") of faint light flashes. The probability of seeing a flash was recorded for light pulses of different intensity. From fitting the observed probability curve it was possible to deduce the visual threshold, which turned out to be in the range of 2–8 photons impinging on the retina. The observations are back to ancient astronomy where we know the flux of photons from distant stars and able to correlate the visibility of a star with the corresponding photon flux.

More precise suitable methods appeared later. Intracellular recordings in electrophysiology appeared by 1950s after introducing glass microelectrodes with tiny thin sharp tips (diameter of about 0.1 μm) (history of electrophysiology is well reviewed in: [67]). These impalement electrodes gave opportunity to insert the sharp tips into a single cell and measure electric properties of cell membranes under certain conditions. This method is very productive to measure kinetics of membrane potential in rod cells under illumination. After the initial recordings with the preparations of retina (e.g. [68]) it was suggested that the main source of electric activity in retina under illumination were rods and cones [69]. The study shifted to individual rod cells [70, 71]; from the other side the use of arrays of extracellular electrodes confirmed that the photoelectric activity of retina is linked to outer segments of rod cells [72]. Application of numerous inhibitors and stimulators together with varying the external medium for rod cells provided plenty of information about the mechanisms of the processes [33, 34]. By the end of the 1970s, with an invention of the patch clamp technique more opportunities become available. Indeed, the technique allows to change the intracellular composition and record ion currents under determined voltages. It helped to decipher the role of cGMP in regulating ion currents [14] and completed the scheme of phototransduction chains and intracellular events.

The other approach was also developed allowing direct measurement of membrane current of a single photoreceptor upon light stimulation [73, 74]. The method,

known as suction electrode, uses tight glass micropipette to monitor the membrane current of the rod cell. One segment of the rod cell is drawn in the micropipette filled with the physiological solution, see Fig. 6.10b. The rod cell is functioning as in vivo, but the current, flowing through the cell membrane, is now re-directed to a low noise ampere meter. In the dark the microelectrode measures the current, caused by continuous transport of ions (Na^+, K^+, Ca^{2+}) through ion channels in the membrane. Once a photon hits the ROS, it isomerizes the rhodopsin pigment and starts a phototransduction cascade, which results in a closure of specific ion channels and prevents ions from entering the cell. Change of the membrane current (typically a few pA) is detected by the suction micropipette. The examples of waveforms of the rod photocurrent at various number of impinging photons are shown in Fig. 6.4.

Methods of delivering regulated number of photons to eye or rod cells also progressed since the end of the 19th century: the parallel or biased advances in (1) optical methods and theory from one side and (2) ways of recording response from rod cells from the other side determined the trajectory of the research.

6.2 Overview of the Earlier Visual Experiments

The first known reported visual experiments are dated back to 1889 [65]. The aim of the research was to determine the sensitivity of eye depending on the colour of light. The light energy was measured by self-made sensitive bolometer, while an observer indicated the visibility of attenuated light ray. Four different observers were chosen for experiments. The conclusions were that sensitivity to green light was about 100 times higher than for red or violet light and the green light sensitivity corresponded to about $3 * 10^{-9}$ erg or $3 * 10^{-16}$ J. Recalculating we assume that about 1,000 photons were the minimal visible number for the experiments, a reasonable initial result taking into account numerous sources of errors described in the paper [65]. Further experiments led to about 35–70 photons [66] or about 40–90 photons as a minimal sensitivity threshold in these experiments [75] (several experimental results are summarised and reviewed in [76]).

It is worth mentioning and describing in more detail the experimental results of Sergey Vavilov (Wawilow) on visual perception obtained in 1930s and 1940s since the results are rather undervalued yet [77–81] (Translation into English of some of his papers is included in the Part 2 of this book). The thoughtful and well-organised experiments included dark preadaptation of eye for about one hour and used uranium glass and several uranium salts to check the level of adaptation. Dark adapted eye was able to see the luminescence of uranium glass. Special fixation point was helpful to set the defined position of eye and direct photons to specific most sensitive part of retina. The excitation of the eye lasted for 0.1 s with further gap for 0.9 s. The observer did not know the presence or absence of excitation by photons. The minimal number of detected photons was not a strict number with sharp threshold, but varied depending on the observer and even changed twice within the

same day for the same observer following physiological conditions. The number was considered as photons impinging on the cornea of eye in the first experiments of 1930s and later on in 1940s as photons absorbed by retina. Plotting the probability of seeing against number of photons helped to determine the visual threshold for retina based on the slope of the curves. The threshold was about 20–40 photons (from 8 to over 45 for different observers) for several series of experiments over 10 years. The source of light was an incandescent light bulb supplied by electric power, the light beam was weakened in a quantitative manner after the green filter to ensure the highest eye sensitivity. Since eye was the most sensitive light detector at the time, eye was also used to detect quantum fluctuations in weak light beams, hence served as a measuring device for precise physical measurements [77–81].

Among classic behavioral experiments on threshold of vision are the works of Hecht and colleagues [76, 82]. The researchers determined the minimal number of detected photons of green-blue range of spectrum as 54–148 and made assumption concerning the number of photons reaching retinal rods. Estimates for absorption and reflection by cornea, absorption by lens and the other parts of eye to around 90% of the initial value allowed to find the minimal threshold of photons sensed by retina: the threshold was from 5 to 15 photons.

Behavioral experiments are very important for understanding general peculiarities of vision and also for setting background for further more detailed visual research. To compare with human visual threshold the behavioral study included even animals, e.g. cats and owls; cat had 6 times lower visual threshold [83], owl also likely had a lower threshold compared to human, while having similar spectral sensitivity [84].

Interesting and highly analytical series of behavioral experiments was carried out with laser source of light [85–87]. Plane polarised light pulse with duration 1 ms from Ar^+ green laser had Poisson distribution of photons. The 1 ms pulse was used for "can see-can not see" trials with four trained male observers. Several options were offered for the observers from (1) reporting positive and negative responses of seeing the light pulse (low false-positive rate) to (2) encouraging them to report on any possible occasion of seeing a light flash (high false-positive rate). Low false-positive rate corresponded to 127–147 photons as minimal number of visible photons impinging on cornea, high false-positive rate gave threshold being 42–82 photons. The obvious conclusion is that reliability and sensitivity are not compatible. Modelling gave numeric parameters: 60% probability of seeing with 1% of false-positive rate gave 147 photons, rise of false-positive rate to 33% decreased the number of photons to 34 [85]. Assessing the experimental data resulted in the threshold at retina from 11 to 32 photons with similar values of dark noise at retina [86]. Moreover, the next important step was to evaluate the role of photon statistics from the light source on the visual perception [87]. Intensity modulation of a Poissonian laser light gave nearly flat distribution with similar number of counts per unit of time instead of peak in Poissonian distribution; it changed the curve for probability of vision for the same energies. At low false-positive rate the corneal threshold increased from 147 to 162; the curves at both high and low false-positive

rates became more shallow [87]. The phenomenon was explained by higher frequency of trials with low number of photons and higher uncertainty compared to Poissonian distrubution. The researchers discussed the ideal untibunched light with sub-Poissonian statistics for potentially getting more information for probability curve and threshold of vision. From one side, these detailed experiments provided further understanding of visual perception depending on (1) noise with different distributions of events in visual system, (2) statistics of photons and (3) false-positive settings [86–88]. From the other side, they obviously pointed to the limitation of behavioral experiments due to high losses in eye and dependence on physiological conditions of observers.

The mainstream of research evidently and inevitably led to complemeting study of isolated rod cells [14, 73, 74, 88–90]. Microelectrode recordings (e.g. [91, 92]) and later both patch clamp [14, 30, 31, 89, 90] and suction electrode [73, 74, 88] techniques were productive for the visual experiments. We will describe the experiments briefly since the further part provides similar data using more controlled source of light. Microelectrode recordings demonstrated hyperpolarisation of rod cells from below 1 mV up to 30 mV after illumination depending on the intensity of the light stimulus [e.g. 91, 93]. Similar dose-response curves with saturation for ion currents were recorded by suction electrode for rods of toad *Bufo marines*. Saturation values for sigmoid curve (logarithmic scale of abscissa for number of photons) of current were around 20 pA, the source of light used was tungsten-iodide lamp [73, 74, 88]. The electric response to dim light was quantised suggesting that an individual rod cell was able to absorb single photons and respond by nearly 1 pA current pulses with quantum efficiency equal to 0.5 ± 0.1 [74]. The experiments also confirmed the spectral sensitivity of rod cells peaking in green light with wavelength about 500 nm [73].

Patch clamp recordings with isolated rod cells added more information about (1) the reversal potential of light-sensitive ion currents indicating to specific cations for the current, (2) properties of light-sensitive noise at high frequencies of recordings and (3) were helpful to measure single photon responses of genetically modified mice rod cells [e.g. 14, 30, 31, 89, 90]. Noisy recordings under dark conditions corresponded to fluctuations in conductance of cyclic nucleotide gated ion channels, light pulse closed these ion channels and noise at the corresponding frequency dropped [90]. Several other components of noise were analysed; it is worth to mention again the large spontaneous fluctuations of dark noise in vertebrate photoreceptors derived from spontaneous isomerisation of rhodopsin, the peaks of current and voltage are similar to single photon responses (reviewed in: [94]). Interestingly, the light-dependent saturation current in frog rods measured by patch clamp was about 25 pA, which is similar to recordings in toad rods by suction electrode [90]. Basic parameters of photocurrents in rods of jawless lampreys also coincided for measurements by suction electrode and using patch clamp, though patch clamp provided more detailed parameters of ion currents [31]. The light sources for the experiments were either tungsten lamps or light-emitting diods (LEDs) of green spectral range, while statistics of photons was not controlled and was not specially measured.

6.3 Interaction of Rod Cells with Classical and Quantum Light Sources

In nature we often deal with flickering lights. Representative examples are observation of blinking stars and firecrackers. However, even if the light appears stable to the eye it still exhibits a variation in the number of photons, known as photon noise. The number of photons at each moment is not strictly constant but it is rather described by a specific statistical function, which depends on the light source. For example, the photon number distribution for a laser obeys Poissonian statistics. For a thermal source (lamp, star, LED) the photon number distribution obeys Bose-Einstein statistics. Examples of two distributions, for the same average photon number are shown in Fig. 6.5. As expected, the distribution for the laser is much narrower than for the thermal source. The photon noise (or photon fluctuations) is caused by the quantized nature of light and it cannot be eliminated by technical means.

Historically, visual experiments were mainly focused on studies of averaged visual responses to repeatable light flashes. Direct impact of photon noise on the vision process was often unnoticed. However, as we shall see later in this Chapter, careful account for statistical properties of the impinging light is crucial for accurate interpretation of visual experiments. Light sources with controllable statistical properties can be engineered using tools and approaches of modern quantum optics.

In experiments conducted at a single photon level impact of photon fluctuations becomes increasingly important. Indeed, in this case the average number of photons becomes comparable or even less than the corresponding standard deviation. The statistical distribution of responses of rod cells was shown to follow the discrete distribution of photons, which confirmed the single photon sensitivity of rod cells. Recently rod cells were interfaced with a specialised light source which produces

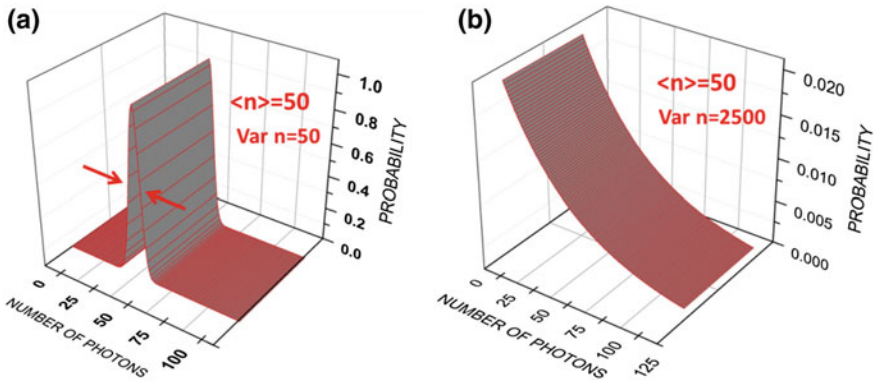

Fig. 6.5 Photon number probability distribution for a coherent (**a**) and a thermal (**b**) light sources. The distributions are plotted at the same value of the average photon number of 50 photons. The variance of the number of photons is much narrower for the coherent state of light

either zero or one photon, but never two photons or more [95]. This provided a direct proof of the single photon sensitivity of rod cells.

6.3.1 Experiments with the Whole Visual System

Baylor et al. studied responses of rod cells to extremely faint optical pulses, causing the cells to absorb only few photons [73, 74]. Experiments revealed remarkable trial-to-trial stability and discretization of cell responses. These findings led to the conclusion on the ability of individual rod cells to detect single photons. The probability distribution of response amplitudes was found to be Poissonian. However, detailed analysis of influence of photon fluctuations on the cell response was out of the scope of those works.

Influence of controllable photon fluctuations on the response of the visual system was first studied in experiments by Teich and colleagues [85–87]. A light source with a super-Poissonian photon probability distribution was used in conventional frequency-of-seeing experiments. The source consisted of a laser and an acousto-optical intensity modulator (AOM). Setting the shape of the driving signal of the AOM allowed precise control over the shape of the photon number distribution. Such a source mimics the cathodoluminescence light, which can be observed as emission from a fluorophore screen bombarded by electrons.

Frequency-of-seeing curves obtained with the super-Poissonian light source were found to be less steep compared to the curves obtained with a Poissonian source. This effect was associated with difference in photon number distributions. Let us consider the two light sources emit the same average number of photons. The photon number distribution for a super-Poissonian source is broader than for the Poissonian one. Hence the probability of emission of pulses with extremely small and extremely large number of photons is higher for the super-Poissonian source. Pulses with low number of photons are unlikely to be detected by the observer. At the same time pulses with high number of photons are detected with almost the same probability as pulses from a Poissonian source. As a result, the overall probability to see the flash is decreased for the light source with the increased variance in the number of the impinging photons.

The obtained results are particularly important in measurements of the visual threshold, which is conventionally obtained from fitting of frequency of seeing curves. The curves obtained in experiments with light sources of different photon statistics will yield different values of the threshold. Hence, a proper account for statistical properties of the light source is absolutely necessary to avoid any inconsistencies in measurements of the threshold.

6.3.2 Experiments with Isolated Rod Cells and Classical Light Sources

Experiments by Teich and colleagues highlighted the importance of careful attention to statistical properties of light sources used in visual studies. However, the role of individual photoreceptors in the observed effect was hindered because a few hundred of rods were simultaneously illuminated and their collective response underwent several intermediate stages of visual processing. In later experiments Sim and colleagues, individual rod cells were stimulated by light sources with various photon statistics [19].

In their experiments Sim and colleagues, used two examples of classical light sources with noticeably different statistical properties, namely coherent and thermal sources. The photon number distribution $P_{\mathrm{ph}}(m)$ for coherent and thermal sources is given by: $P_{\mathrm{coh}}(m) = \frac{\langle m\rangle^m e^{-\langle m\rangle}}{m!}$, $P_{\mathrm{th}}(m) = \frac{\langle m\rangle^m}{(1+\langle m\rangle)^{m+1}}$, respectively, where $\langle m\rangle$ is an average number of photons. The statistics of the rod cell response can be derived using a photon counting model. In the model it was assumed, that (1) once the rhodopsin is isomerized, the response occurs with almost unity probability, (2) responses to individual photoisomerizations are additive and (3) responses have a standard Gaussian shape. The theoretical analysis follows three steps:

1. For a given photon distribution $P_{\mathrm{ph}}(m)$, the probability of excitation of n rhodopsin molecules is given by Mandel's formula:

$$P_I(n) = \sum_{m=1}^{\infty} \binom{m}{n} \eta^n (1-\eta)^{m-n} P_{\mathrm{ph}}(m),$$

   where η is an overall quantum efficiency of photodetection.
2. Probability for observing a cell response with an amplitude A is given by the average over responses to individual isomerizations:

$$P(A) = \sum_{n=0}^{\infty} \frac{1}{\sqrt{2\pi n\sigma^2}} \exp\left(-\frac{(A-nA_0)^2}{2n\sigma^2}\right) P_I(n),$$

   where A_0 is the average amplitude of the response to single isomerization, and σ is its standard deviation.
3. To account for saturation of the response, caused by closure of the all the ion channels in the cell membrane, $P(A)$ is truncated at the saturation amplitude A_{s}:

$$P_{\mathrm{S}}(A) = \begin{cases} P(A), & \text{if } A < A_{\mathrm{s}} \\ 1 - \int_0^{A_{\mathrm{s}}} P(A)\mathrm{d}A & \text{if } A = A_{\mathrm{s}} \\ 0 & \text{if } A > A_{\mathrm{s}} \end{cases}$$

From the obtained $P_S(A)$ the k-th statistical moment of the response amplitude can be found: according to definition $\langle A^k \rangle = \int A^k P_S(A) \mathrm{d}A$. The signal to noise ratio (SNR) is defined as $\mathrm{SNR} = \sqrt{\langle A \rangle^2 / \mathrm{Var}\, A}$, where variance is $\mathrm{Var}A = \langle A^2 \rangle - \langle A \rangle^2$. If the amplitude of each response is measured along with a number of photons in each pulse K, the Glauber's second order correlation function $g^{(2)}$, given by $g^{(2)} = \langle AK \rangle / \langle A \rangle \langle K \rangle$, can be obtained [96].

In the experiment two light sources (coherent and thermal) were realized using the same laser (a frequency doubled Nd:YAG laser, modulated by a mechanical shutter) with the wavelength of 532 nm. In the experiment with the coherent source, the laser beam was split on a 50/50 beamsplitter and then directly coupled into two optical fibers, one of which was used for stimulation of the cell and another one was directed to a single photon avalanche photodiode (APD). In the experiment with the thermal source, the same laser beam was first scattered by a rotating ground glass disk, and then, a single scattered speckle was coupled into the fiber. The intensity of the speckle at different orientations of the disc follows the thermal distribution [97].

Dependence of the average amplitude of cell response on the number of impinging photons for the two sources is shown in Fig. 6.6. The curve is much steeper for the coherent source than for the thermal one. This effect can be understood from the analysis of experimental probability histograms of response amplitudes, shown in Fig. 6.7. For stimulation with relatively weak pulses the rod cell behaves as a linear photodetector and the histograms reflect the statistics of light pulses, see Fig. 6.7a, b (red bars). However, once the number of impinging photons is sufficient to cause saturation of the cell response, significant variations are observed. For the coherent source the photon probability distribution can be approximated by a Gaussian function, which is well localized around its average value. In this case the majority of rod responses will be "concentrated" around the saturation amplitude A_s, see Fig. 6.7a (black bars). For the thermal source the photon probability distribution is a decaying exponential function, and even if the average number of photons is large, there is always a non-vanishing probability for emission of pulses with just a few photons. Hence some responses will have amplitudes well below A_s, see Fig. 6.7b (black bars). Because of contribution of such events, the average amplitude becomes smaller and as a result, the cell response is less steep. Remarkably, obtained results are consistent with earlier findings of frequency of seeing experiments by Teich and colleagues, suggesting that responses of isolated rod cells are at the basis of those effects [85–87].

Saturation also reveals itself in dependencies of the signal-to-noise ratio (SNR), see Fig. 6.8. For stimulation with weak pulses, the cell response is linear and it reflects the statistics of the light source: $\mathrm{Var}A = \langle A \rangle \rightarrow \mathrm{SNR} = \sqrt{\langle A \rangle}$ for the coherent source, and $\mathrm{Var}A = \langle A \rangle^2 \rightarrow \mathrm{SNR} = 1$ for the thermal source. In the saturation regime the cell most likely to return responses with amplitudes equal to A_s, which leads to reduction of the variance and growth of the SNR for both sources. This is confirmed by numerical simulations, see lines in Fig. 6.8.

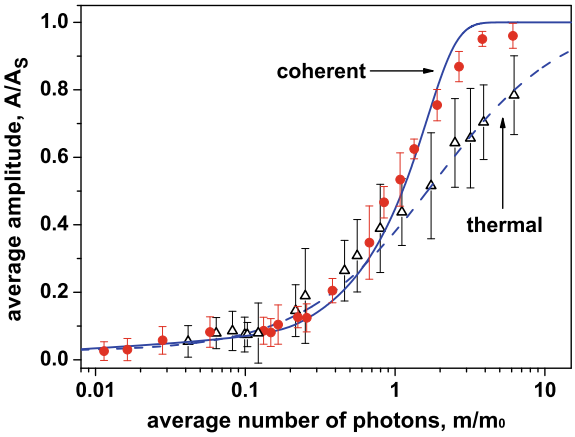

Fig. 6.6 Dependence of the average amplitude of the rod response on the average number of photons for coherent (red circles, solid line) and thermal (black triangles, dashed line) sources. Amplitudes are normalized for a saturation amplitude A_s, and the number of photons is normalized to the number of photons in the coherent pulse m_0 which initiated a response of a half saturation amplitude ($m_0 \approx 550$–2500 photon per pulse (number of photons is not adjusted for the efficiency of photon delivery to the cell)). The curves are averaged over 6 cells from 6 different animals and error bars show ±s.d. Lines show numerical calculations according to the photon counting model. The dependencies show different trends due to differences in photon statistics of the light sources. The difference becomes especially noticeable when the response is close to the saturation. From [19]

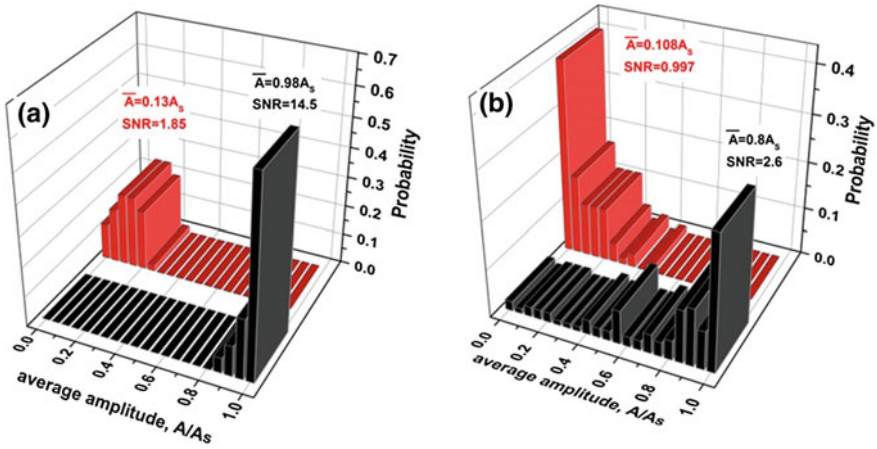

Fig. 6.7 Probability histograms of normalized amplitudes measured for coherent (**a**) and pseudothermal (**b**) sources at different values of the average amplitude of cell response (normalized to the saturation amplitude A_s), shown with the corresponding SNR values. Red and black bars correspond to linear and close-to-saturation regime of cell response, respectively. Adapted from [19]

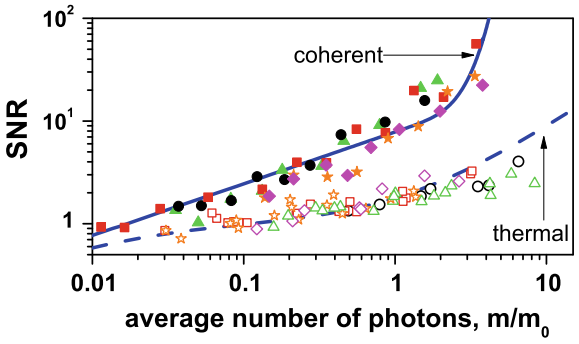

Fig. 6.8 Dependence of the signal-to-noise ratio (SNR) on the average number of photons normalised to the number of photons in the coherent pulse m_0 which initiated a response of a half saturation amplitude. Closed symbols, solid line show the results for the coherent source. Open symbols, dashed line show results for the thermal source. Different symbol shapes correspond to data obtained from different cells. Lines show numerical calculations according to the photon counting model. Adapted from [19]

It is also interesting to analyse the trend of the second order correlation function $g^{(2)}$, see Fig. 6.9. When the rod cell is stimulated by a coherent source $g^{(2)}$ is equal to 1 and it does not depend on the number of photons. This result is expected because after the beam-splitter photons impinging on the cell and on the APD are not correlated [96]. For the thermal source $g^{(2)}$ decreases with the increase of the number of photons from theoretical value of 2 to 1. In the saturation regime the cell consistently produces responses with amplitudes equal to A_s. The response amplitude can be traced out of the averaging $\langle AK\rangle \approx A_s\langle K\rangle$ in the nominator of $g^{(2)}$, which results in the asymptotic value of $g^{(2)} = 1$.

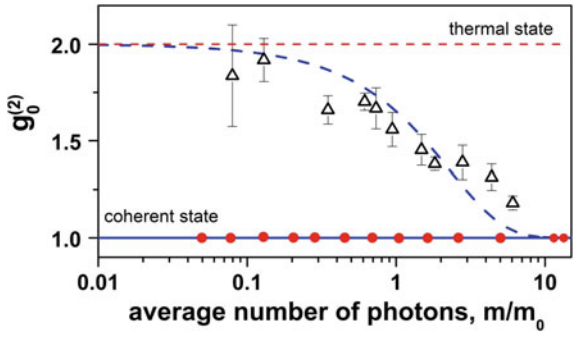

Fig. 6.9 Dependence of the second order correlation function $g_0^{(2)}$ on the average number of photons for coherent (red circles, solid line) and thermal (black triangles, dashed line) sources. Lines show numerical calculations according to the photon counting model. Saturation of the cell response leads to the decrease of $g_0^{(2)}$ for the thermal source, while $g_0^{(2)}$ stays constant for the coherent source. Error bars show ±s.d. Adapted from [19]

6.3.3 *Interfacing Rod Cells with a True Single Photon Source*

Behavioural and electrophysiological experiments evidenced that rod cells are capable to respond to light at the level of single photons [25, 29]. In those studies conventional light sources such as lamps, lasers, and LEDs were used. As discussed above, such sources exhibit fundamental fluctuations in the number of emitted photons. These fluctuations become crucial at ultra-low intensities of light pulses. In this case, variance of the number of emitted photons becomes comparable or even larger than the mean value. Hence, the single photon sensitivity of rod cells can only be inferred from the statistical analysis. Moreover, the uncertainty in the number of photons, impinging on the cell, hinders accurate characterization of underlying bio-chemical mechanisms of the photo-transduction. The intrinsic physiological noise of the cell cannot be distinguished from the noise due to fluctuations of light stimuli. A feasible way to address these problems is to use a specially engineered light source, which produces pulses with given number of photons down to single photon level. This experiment was recently realized in the work of Phan and colleagues [95].

Considerable interest is focused on the development of single photon sources for the purposes of secure communication and quantum computing. Phan and colleagues, engineered a single photon source which allows studying interaction of single photons with a biological object. The single photon source is based on a process of spontaneous parametric down conversion (SPDC) [98]. In the SPDC a fraction of a laser pulse (pump), propagating in a non-linear optical crystal, is converted into a pair of photons (signal and idler), which obey conservation of energy and momentum:

$$\omega_{\mathrm{p}} = \omega_{\mathrm{s}} + \omega_{\mathrm{i}} \quad k_{\mathrm{p}} = k_{\mathrm{s}} + k_{\mathrm{i}},$$

where $\omega_{\mathrm{p,\,s,\,i}}$ and $k_{\mathrm{p,s,i}}$ are frequencies and wave vectors of pump, signal, and idler photons, respectively. SPDC is a probabilistic process, but conservation laws guarantee that the signal and idler photons are emitted simultaneously and in strictly defined directions. In the experiment, signal and idler photons were created from a pulsed UV-laser with $\lambda_{\mathrm{p}} = 266$ nm. The photons were of the same wavelengths of $\lambda_{\mathrm{s}} = \lambda_{\mathrm{i}} = 532$ nm, which were chosen to maximize the absorption by the cell. The signal and idler photons travelled in two different directions, which form an angle of $\pm 3^{\circ}$ to the direction of the pump beam, see Fig. 6.10. The pump power was adjusted to minimise the chance of creation of more than one pair from a single pump pulse.

Correlation between signal and idler photons can be readily exploited in generation of single photon pulses. A single-photon avalanche photodiode (APD) was put in the signal beam, and a fast optical shutter (acousto-optical modulator) in the idler beam, see Fig. 6.10. The APD output was used to trigger opening of the shutter in the idler beam. Once the signal photon was detected by the APD,

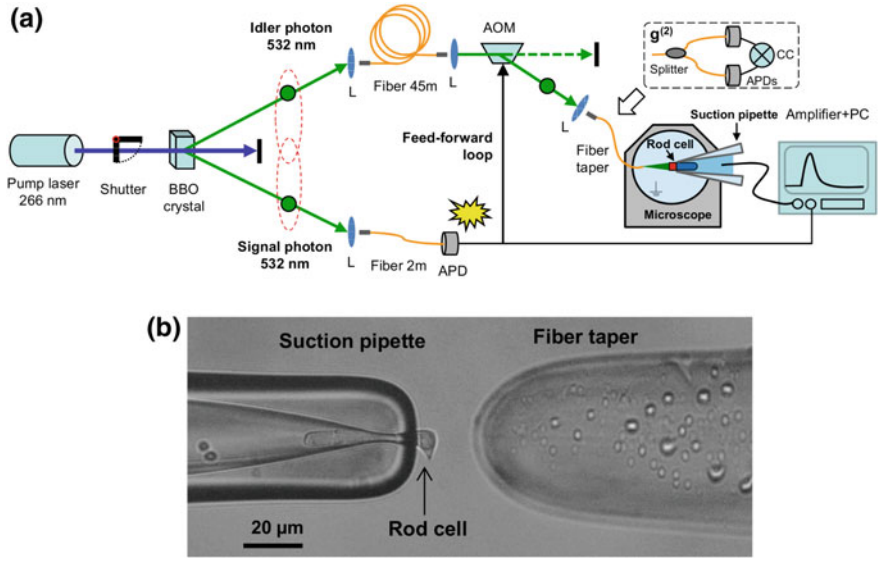

Fig. 6.10 **a** Experimental setup for single photon stimulation of retinal rod cells. A pulsed laser at 266 nm pumps a Beta barium borate (BBO) crystal, where spontaneous parametric down conversion (SPDC) occurs. Signal and idler photons are emitted at 532 nm. Signal photon is detected by the avalanche photodiode (APD) and it triggers an acousto-optical modulator (AOM) in the idler arm. The idler photon travels in a 45 m long fiber and gets deflected by the AOM. It is then addressed to a tapered fiber, pointing at the rod cell. Excitation of the rod cell is recorded with the suction electrode technique. Inset shows a setup used for the measurement of the correlation function of the single photon consisting of a 50/50 beam splitter and two APDs connected to a coincidence circuit. **b** Microscope image shows position of the rod cell in the recording pipette interfaced with a taper of the optical fiber. Adapted from [95]

the shutter opened for a brief period of time, during which the idler photon passed through it. The idler photon was delayed by an optical fiber, to compensate for electronic delays, and a time jitter of the shutter. In case if the APD did not detect a signal photon the shutter remained closed and no light pulse was sent to the cell. Thus, observation of a photocount of the APD in the signal beam heralded presence of a single photon in the idler beam. The heralded single photon was then directed to the rod cell in the recording pipette via an optical fiber [99].

Single photon sources are conventionally assessed with the second order intensity correlation function $g^{(2)}$. In the experiment $g^{(2)}$ of heralded photons was measured using a 50/50 beamsplitter and two APDs with their outputs connected to a coincidence circuit, see inset Fig. 6.10. The source yielded $g^{(2)} = 0.08 \pm 0.06$, which means that the probability of obtaining a multiphoton event is 12.5 times less, compared to the coherent source with $g^{(2)} = 1$.

Rod cells were isolated from dark adapted retinas of frogs *Xenopus laevis*. Real-time monitoring of the membrane current was realized using the suction electrode technique [73, 74]. Waveforms, accompanied by the APD photocounts,

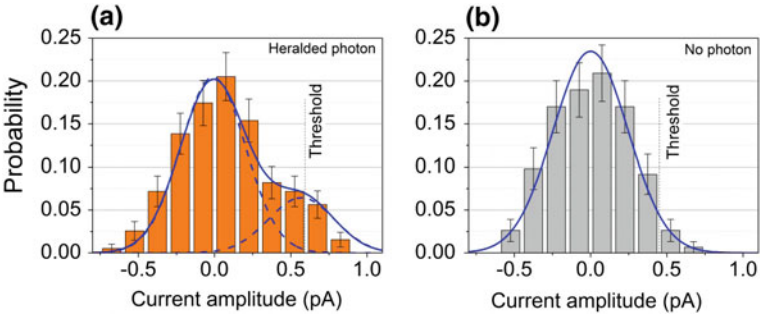

Fig. 6.11 **a** Probability distribution of cell electric response amplitudes when the APD heralds a presence of a single photon and **b** when there is no heralding signal (dark noise). Solid lines are Gaussian fits. The vertical dashed lines indicate the threshold level ($A \geq 0.45$ pA) for calculation of single-photon responses. Error bars show ±s.d. Adapted from [95]

were used to analyse single photon responses. Waveforms, acquired in the absence of the APD photocounts, are used to analyse the dark noise.

Probability histogram of waveform amplitudes for the case, when the APD heralds the presence of a single photon, is shown Fig. 6.11a (orange bars). It shows two distinctive peaks: a non-response peak (centered about 0 pA) and a single photon response peak (centered about 0.6 pA). Histograms of the dark noise for the same cell is plotted in Fig. 6.11b (grey bars). It reveals few *single photon-like* dark noise responses, which are less frequent than in case of single photon stimulation.

From the amplitude histogram, a criterion-based method is established to identify single-photon responses. Waveforms with amplitudes higher than the criterion level are categorized as "*single photon responses*", and lower than the criterion level as "*no responses*". Based on discretisation of the histogram in Fig. 6.11a, the criterion level is selected at 0.45 pA.

Probability of occurrence of single photon responses, which satisfy the above mentioned criteria, is consistently higher for single photon stimulation, than for the dark noise, see Fig. 6.12. Thus responsiveness of the cell to stimuli, produced by the heralded single photon source is clearly justified.

Averaged waveform of single photon responses is shown in Fig. 6.13a. It shows consistent amplitude, time-to-peak, and duration. Averaged zero-photon response does not show any distinctive shape and appear almost flat, see Fig. 6.13b. The parameters of the waveforms for ten different cells from ten different animals, are summarized in Table 2. Cell-to-cell variations could be attributed to differences in intrinsic capabilities of single photon detection, different resistances of the suction electrodes, and different efficiencies of light coupling. Nevertheless, the results allow clear identification of amplitudes of single photon responses for the majority of studied cells within the range 0.5–0.7 pA.

Quantum efficiency (QE) of the rod cell is an important parameter, which characterizes its ability to respond to light. QE can be defined similar to man-made single photon detectors as a coefficient between the number of responses and the

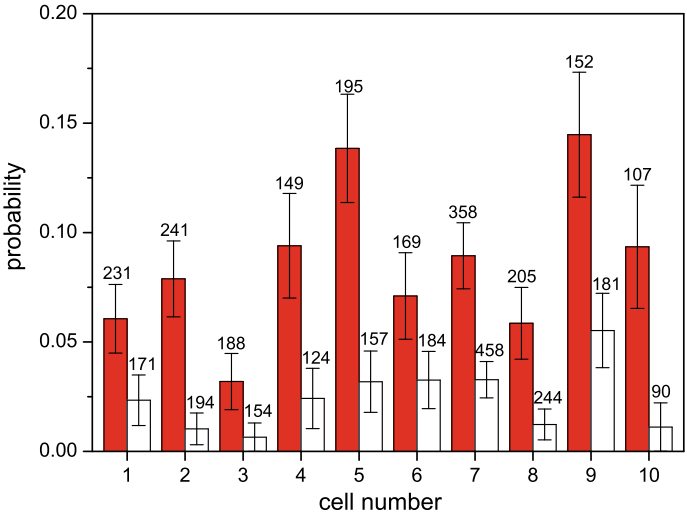

Fig. 6.12 Probability of the occurrence of single-photon responses, satisfying the criterion ($A \geq 0.45$ pA), when the APD heralds a single photon (red bars) and for the dark noise (white bars). Labels correspond to the number of experimental trials. Error bars show ±s.d. Adapted from [95]

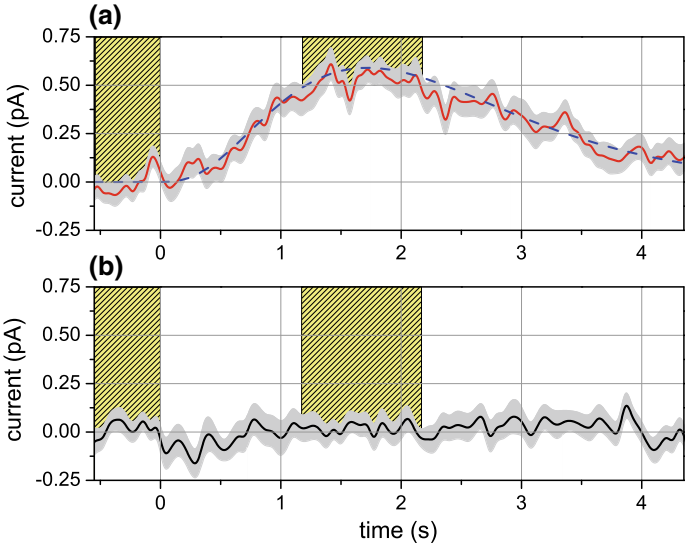

Fig. 6.13 **a** Representative average waveform of the cell responses (cell # 5 in Fig. 6.12) to single photons (red solid line), and **b** of non-responses (bandwidth 20 Hz, 27 traces). Blue dashed line in (**a**) is a theoretical curve based on the impulse response of the Poisson filter. Shutter in the pump beam is opened for a period of 100 ms at $t = 0$. Yellow shaded regions indicate widths of time windows for calculation of waveform amplitudes. Grey shaded regions in (**a**, **b**) show ±s.e.m. Adapted from [95]

Table 2 Parameters of single photon responses for rod cells from dark adapted retinas of frogs *Xenopus laevis** [95]

Cell #	Amplitude, pA	Time to peak, s	Full width at the level of half amplitude, s	Number of traces
1	0.54 ± 0.02	2.7 ± 0.2	2.8 ± 0.1	14
2	0.58 ± 0.02	1.8 ± 0.1	2.2 ± 0.1	19
3	0.59 ± 0.03	2.9 ± 0.2	3.6 ± 0.2	6
4	0.57 ± 0.02	0.7 ± 0.1	1.0 ± 0.1	14
5	0.65 ± 0.03	1.7 ± 0.1	2.5 ± 0.1	27
6	0.57 ± 0.03	1.9 ± 0.1	2.3 ± 0.2	12
7	0.59 ± 0.02	2.8 ± 0.1	2.4 ± 0.15	32
8	0.60 ± 0.05	1.8 ± 0.1	2.0 ± 0.1	12
9	0.65 ± 0.03	0.7 ± 0.1	1.6 ± 0.1	22
10	0.60 ± 0.04	0.95 ± 0.15	1.3 ± 0.1	10

*Values are the mean ± s.e.m.

number of impinging photons. Let us consider that N photon pairs were emitted from the SPDC crystal. The number of photons, detected by the APD in the signal beam, is $n_{\mathrm{APD}} = \eta_{\mathrm{APD}} \mathrm{N}$, where η_{APD} is the APD quantum efficiency. After that, n_{APD} trigger pulses will be sent to the optical shutter in the idler arm. The corresponding number of photons detected by the cell is $n_{\mathrm{Cell}} = \eta_{\mathrm{Cell}} \eta_{\mathrm{APD}}$, where η_{Cell} is the unknown quantum efficiency of the cell (here, for the moment, we neglect optical losses in the idler beam). Form the above η_{Cell} can be found as a ratio of the two directly measured experimental values, $\eta_{\mathrm{Cell}} = n_{\mathrm{Cell}} / n_{\mathrm{APD}}$. In contrast to conventional techniques of QE calibration, this method does not require the use of any pre-calibrated devices [100]. From data in Fig. 6.12, and taking into account optical losses in the idler channel, and the dark noise, the average value of the QE for ten studied cells is $\eta_{\mathrm{Cell}} = 29 \pm 4.7\%$. This value is in good agreement with earlier physiological studies for *Xenopus*.

The experiment with a true single photon source provided a conclusive proof of single photon sensitivity of rod cells. It also demonstrated application of the reference-free calibration technique to measurement of the cell's QE.

6.4 Conclusions and Future Perspectives

Fast progress in molecular biology and protein chemistry offers new ways of measuring the voltage output from rod cells and novel means to manipulate the phototransduction mechanisms. Recent development of voltage-sensitive fluorescent proteins and dyes (reviewed in: [101]) could be useful for measurements of membrane potential in rod cells under illumination. Potentially the red or near infra-red fluorescent proteins [102], which do not overlap in their excitation and

emission properties with spectral sensitivity of rod cells and fused with voltage-sensitive sensor might be helpful in elucidating the distribution of membrane potential in rod cells under dark conditions and after pulse of photons. The other already used means is to modify or correct elements of phototransduction cascades. Recently adeno-associated viral delivery of genes proved to be effective for functional expression of proteins in human and mice retinal photoreceptors [103].

From the optical perspective, an interesting development could be studies of interaction of rod cells with pulses carrying precise number of photons (more than one). Following the proposal by Teich and colleagues, such an experiment would allow characterizing statistical properties of distinctive steps in the phototransduction in much more precise way, as compared to Poissonian light sources [85–87]. It may also lead to direct observation of quantum properties, such as entanglement and squeezing, possibly with naked eyes [104].

References

1. J.E. Dowling, *The Retina: An Approachable Part of the Brain* (Belknap Press of Harvard University Press, Cambridge, MA, 2012). Revised Edition
2. C.R. Braekevelt, S.A. Smith, B.J. Smith, Fine structure of the retinal photoreceptors of the barred owl (Strix varia). Histol. Histopathol. **11**(1), 79–88 (1996)
3. M. Joseph, A. Corless, Minimum diameter limit for retinal rod outer segment disks. *Development of Order in the Visual System*, ed. by S.R. Hilfer et al. (Springer, New York Inc., 1986), pp. 127–142
4. K. Palczewski, G protein-coupled receptor rhodopsin. Annu. Rev. Biochem. **75**, 743–767 (2006)
5. M.L. Woodruff, M.D. Bownds, Amplitude, kinetics, and reversibility of a light-induced decrease in guanosine 3′,5′-cyclic monophosphate in frog photoreceptor membranes. J. Gen. Physiol. **73**(5), 629–653 (1979)
6. H.W. Choe, Y.J. Kim, J.H. Park, T. Morizumi, E.F. Pai, N. Krauss, K.P. Hofmann, P. Scheerer, O.P. Ernst, Crystal structure of metarhodopsin II. Nature **471**, 651–655 (2011)
7. K. Palczewski, T. Kumasaka, T. Hori, C.A. Behnke, H. Motoshima, B.A. Fox, I. Le Trong, D.C. Teller, T. Okada, R.E. Stenkamp et al., Crystal structure of rhodopsin: a G protein-coupled receptor. Science **289**, 739–745 (2000)
8. L. Stryer, Exploring light and life. J. Biol. Chem. **287**, 15164–15173 (2012)
9. T.D. Lamb, Gain and kinetics of activation in the G-protein cascade of phototransduction. Proc. Natl. Acad. Sci. U.S.A. **93**, 566–570 (1996)
10. T.D. Lamb, E.N. Pugh Jr., Phototransduction, dark adaptation, and rhodopsin regeneration the proctor lecture. Invest. Ophthalmol. Vis. Sci. **47**, 5138–5152 (2006)
11. E.N. Pugh Jr., T.D. Lamb, Cyclic GMP and calcium: the internal messengers of excitation and adaptation in vertebrate photoreceptors. Vis. Res. **30**, 1923–1948 (1990)
12. R.H. Cote, M.A. Brunnock, Intracellular cGMP concentration in rod photoreceptors is regulated by binding to high and moderate affinity cGMP binding sites. Biol. Chem. **268** (23), 17190–17198 (1993)
13. X. Zhang, R.H. Cote, cGMP signaling in vertebrate retinal photoreceptor cells. Front Biosci. **10**, 1191–1204 (2005)

14. E.E. Fesenko, S.S. Kolesnikov, A.L. Lyubarsky, Induction by cyclic GMP of cationic conductance in plasma membrane of retinal rod outer segment. Nature **313**, 310–313 (1985)
15. W.H. Cobbs, E.N. Pugh Jr., Cyclic GMP can increase rod outer-segment light-sensitive current 10-fold without delay of excitation. Nature **313**, 585–587 (1985)
16. K. Matulef, W.N. Zagotta, Cyclic nucleotide-gated ion channels. Annu. Rev. Cell Dev. Biol. **19**, 23–44 (2003)
17. R.R. Birge, Nature of the primary photochemical events in rhodopsin and bacteriorhodopsin. Biochim. Biophys. Acta **1016**, 293–327 (1990)
18. B.K.-K. Fung, J.B. Hurley, L. Stryer, Flow of information in the light-triggered cyclic nucleotide cascade of vision. Proc. Natl. Acad. Sci. U.S.A. **78**, 152–156 (1981)
19. N. Sim, M.F. Cheng, D. Bessarab, C.M. Jones, L.A. Krivitsky, Measurement of photon statistics with live photoreceptor cells. Phys. Rev. Lett. **109**, 113601 (2012)
20. M.E. Burns, E.N. Pugh Jr., Lessons from photoreceptors: turning off G-protein signaling in living cells. Physiology (Bethesda) **25**, 72–84 (2010)
21. C.M. Krispel, D. Chen, N. Melling, Y.J. Chen, K.A. Martemyanov, N. Quillinan, V.Y. Arshavsky, T.G. Wensel, C.K. Chen, M.E. Burns, RGS expression rate-limits recovery of rod photoresponses. Neuron **51**, 409–416 (2006)
22. C.K. Chen, M.L. Woodruff, F.S. Chen, D. Chen, G.L. Fain, Background light produces a recoverin-dependent modulation of activated-rhodopsin lifetime in mouse rods. J. Neurosci. **30**, 1213–1220 (2010)
23. W.H. Cobbs, E.N. Pugh Jr., Kinetics and components of the flash photocurrent of isolated retinal rods of the larval salamander, *Ambystoma tigrinum*. J. Physiol. **394**, 529–572 (1987)
24. P. Bisegna, G. Caruso, D. Andreucci, L. Shen, V.V. Gurevich, H.E. Hamm, E. DiBenedetto, Diffusion of the second messengers in the cytoplasm acts as a variability suppressor of the single photon response in vertebrate phototransduction. Biophys. J. **94**, 3363–3383 (2008)
25. F. Rieke, D.A. Baylor, Origin of reproducibility in the responses of retinal rods to single photons. Biophys. J. **75**, 1836–1857 (1998)
26. U.B. Kaupp, R. Seifert, Cyclic nucleotide-gated ion channels. Physiol. Rev. **82**(3), 769–824 (2002)
27. E. Eismann, F. Müller, S.H. Heinemann, U.B. Kaupp, A single negative charge within the pore region of a cGMP-gated channel controls rectification, Ca2+ blockage, and ionic selectivity. Proc. Natl. Acad. Sci. U.S.A. **91**(3), 1109–1113 (1994)
28. K.W. Yau, D.A. Baylor, Cyclic GMP activated conductance of retinal photoreceptor cells. Annu. Rev. Neurosci. **12**, 289–327 (1989)
29. F. Rieke, D.A. Baylor, Single photon detection by rod cells of the retina. Rev. Mod. Phys. **70**, 1027–1036 (1998)
30. T. Doan, A. Mendez, P.B. Detwiler, J. Chen, F. Rieke, Multiple phosphorylation sites confer reproducibility of the rod's single-photon responses. Science **313**, 530–533 (2006). PMID: 16873665, http://dx.doi.org/10.1126/science.1126612
31. A.W. Azevedo, T. Doan, H. Moaven, I. Sokal, F. Baameur, S.A. Vishnivetskiy, K.T. Homan, J.J. Tesmer, V.V. Gurevich, J. Chen, F. Rieke, C-terminal threonines and serines play distinct roles in the desensitization of rhodopsin, a G protein-coupled receptor. Elife **4** (2015). https://doi.org/10.7554/elife.05981
32. V. Torre, H.R. Matthews, T.D. Lamb, Role of calcium in regulating the cyclic GMP cascade of phototransduction in retinal rods. Proc. Natl. Acad. Sci. U.S.A. **83**(18), 7109–7113 (1986)
33. M. Capovilla, L. Cervetto, V. Torre, The effect of phosphodiesterase inhibitors on the electrical activity of toad rods. J. Physiol. **343**, 277–294 (1983)
34. M. Capovilla, L. Cervetto, V. Torre, Effects of changing external potassium and chloride concentrations on the photoresponses of Bufo bufo rods. J. Physiol. **307**, 529–551 (1980)
35. E.N. Pugh Jr., T.D. Lamb, Amplification and kinetics of the activation steps in phototransduction. Biochim. Biophys. Acta **1141**(2–3), 111–149 (1993)
36. D.A. Baylor, B.J. Nunn, J.L. Schnapf, The photocurrent, noise and spectral sensitivity of rods of the monkey Macaca fascicularis. J. Physiol. **357**, 575–607 (1984)

37. S. Asteriti, S. Grillner, L. Cangiano, A Cambrian origin for vertebrate rods. eLife **4**, e07166 (2015). https://doi.org/10.7554/elife.07166
38. J.R. Sanes, S.L. Zipursky, Design principles of insect and vertebrate visual systems. Neuron **66**(1), 15–36 (2010). https://doi.org/10.1016/j.neuron.2010.01.018
39. C. Montell, Visual transduction in *Drosophila*. Annu. Rev. Cell Dev. Biol. **15**, 231–268 (1999)
40. C. Montell, *Drosophila* visual transduction. Trends Neurosci. **35**, 356–363 (2012)
41. R.C. Hardie, M. Juusola, Phototransduction in *Drosophila*. Curr. Opin. Neurobiol. **34C**, 37–45 (2015)
42. R.C. Hardie, Phototransduction in Drosophila melanogaster. J. Exp. Biol. **204**(Pt 20), 3403–3409 (2001)
43. A. Auerbach, F. Sachs, Flickering of a nicotinic ion channel to a subconductance state. Biophys. J. **42**(1), 1–10 (1983)
44. O. Alvarez, C. Gonzalez, R. Latorre, Counting channels: a tutorial guide on ion channel fluctuation analysis. Adv. Physiol. Educ. **26**(1–4), 327–341 (2002)
45. I. Lestas, G. Vinnicombe, J. Paulsson, Fundamental limits on the suppression of molecular fluctuations. Nature **467**, 174–178 (2010)
46. D.G. Spiller, C.D. Wood, D.A. Rand, M.R. White, Measurement of single-cell dynamics. Nature **465**, 736–745 (2010)
47. P.N. Steinmetz, R.L. Winslow, Optimal detection of flash intensity differences using rod photocurrent observations. Neural Comput. **11**(5), 1097–1111 (1999)
48. R.A. Yotter, D.M. Wilson, A review of photodetectors for sensing light-emitting reporters in biological systems. IEEE Sens. J. **3**, 288–303 (2003)
49. G.N. Gol'tsman, O. Okunev, G. Chulkova, A. Lipatov, A. Semenov, K. Smirnov, B. Voronov, A. Dzardanov, Picosecond superconducting single-photon optical detector. Appl. Phys. Lett. **79**(6), 705–707 (2001)
50. M. Dandin, P. Abshire, High signal-to-noise ratio avalanche photodiodes with perimeter field gate and active readout. IEEE Electron Device Lett. **33**(4), 570–572 (2012)
51. K. Kolb, Signal-to-noise ratio of Geiger-mode avalanche photodiode single-photon counting detectors. Opt. Eng. **53**(8), 081904 (2014)
52. J.E. Sulston, E. Schierenberg, J.G. White, J.N. Thomson, The embryonic cell lineage of the nematode Caenorhabditis elegans. Dev. Biol. **100**(1), 64–119 (1983)
53. A.S. Chiang, C.Y. Lin, C.C. Chuang, H.M. Chang, C.H. Hsieh, C.W. Yeh, C.T. Shih, J. J. Wu, G.T. Wang, Y.C. Chen, C.C. Wu, G.Y. Chen, Y.T. Ching, P.C. Lee, C.Y. Lin, H.H. Lin, C.C. Wu, H.W. Hsu, Y.A. Huang, J.Y. Chen, H.J. Chiang, C.F. Lu, R.F. Ni, C.Y. Yeh, J.K. Hwang, Three-dimensional reconstruction of brain-wide wiring networks in Drosophila at single-cell resolution. Curr. Biol. **21**(1), 1–11 (2011)
54. L. Chittka, J. Niven, Are bigger brains better? Curr. Biol. **19**, R995–R1008 (2009)
55. S. Herculano-Houzel, The remarkable, yet not extraordinary, human brain as a scaled-up primate brain and its associated cost. Proc. Natl. Acad. Sci. U.S.A. **109**(Suppl 1), 10661–10668 (2012)
56. S.M. Wu, Synaptic transmission in the outer retina. Annu. Rev. Physiol. **56**, 141–168 (1994)
57. W. Bialek, W.G. Owen, Temporal filtering in retinal bipolar cells. Elements of an optimal computation? Biophys. J. **58**(5), 1227–1233 (1990)
58. H. Markram, E. Muller, S. Ramaswamy, M.W. Reimann, M. Abdellah, C.A. Sanchez, A. Ailamaki, L. Alonso-Nanclares, N. Antille, S. Arsever, G.A. Kahou, T.K. Berger, A. Bilgili, N. Buncic, A. Chalimourda, G. Chindemi, J.D. Courcol, F. Delalondre, V. Delattre, S. Druckmann, R. Dumusc, J. Dynes, S. Eilemann, E. Gal, M.E. Gevaert, J.P. Ghobril, A. Gidon, J.W. Graham, A. Gupta, V. Haenel, E. Hay, T. Heinis, J.B. Hernando, M. Hines, L. Kanari, D. Keller, J. Kenyon, G. Khazen, Y. Kim, J.G. King, Z. Kisvarday, P. Kumbhar, S. Lasserre, J.V. Le Bé, B.R. Magalhães, A. Merchán-Pérez, J. Meystre, B.R. Morrice, J. Muller, A. Muñoz-Céspedes, S. Muralidhar, K. Muthurasa, D. Nachbaur, T.H. Newton, M. Nolte, A. Ovcharenko, J. Palacios, L. Pastor, R. Perin, R. Ranjan, I. Riachi, J.R. Rodríguez, J.L. Riquelme, C. Rössert, K. Sfyrakis, Y. Shi, J.C. Shillcock, G. Silberberg, R.

Silva, F. Tauheed, M. Telefont, M. Toledo-Rodriguez, T. Tränkler, W. Van Geit, J.V. Díaz, R. Walker, Y. Wang, S.M. Zaninetta, J. DeFelipe, S.L. Hill, I. Segev, F. Schürmann, Reconstruction and simulation of neocortical microcircuitry. Cell **163**(2), 456–492 (2015)
59. R.G. Boothe, *Perception of the Visual Environmen.* Psychology (Springer Science & Business Media, 2001), 408 pages. ISBN: 978-0-387-98790-3 (Print) 978-0-387-21650-8 (Online)
60. A.P. Sampath, F. Rieke, Selective transmission of single photon responses by saturation at the rod-to-rod bipolar synapse. Neuron **41**(3), 431–443 (2004)
61. D. Attwell, S. Borges, S.M. Wu, M. Wilson, Signal clipping by the rod output synapse. Nature **328**(6130), 522–524 (1987)
62. S. Barnes, V. Merchant, F. Mahmud, Modulation of transmission gain by protons at the photoreceptor output synapse. Proc. Natl. Acad. Sci. U.S.A. **90**(21), 10081–10085 (1993)
63. A.J. Mercer, W.B. Thoreson, The dynamic architecture of photoreceptor ribbon synapses: cytoskeletal, extracellular matrix, and intramembrane proteins. Vis. Neurosci. **28**(6), 453–471 (2011)
64. A. Bharioke, D.B. Chklovskii, Automatic adaptation to fast input changes in a time-invariant neural circuit. PLoS Comput. Biol. **11**(8), e1004315 (2015). https://doi.org/10.1371/journal.pcbi.1004315
65. S.P. Langley, The bolometer and radiant energy, in *Proceedings of the American Academy of Arts and Science*, vol. 16 (American Academy of Arts & Sciences, May 1880–Jun 1881), pp. 342–358. https://doi.org/10.2307/25138616, http://www.jstor.org/stable/25138616
66. J. von Kries, J.A.E. Eyster, Über die zur Erregung des Sehorgans efforderlichen Energiemenzen. Z. Sinnesphysiol. **41**, 373–394 (1907)
67. A. Verkhratsky, O.A. Krishtal, O.H. Petersen, From Galvani to patch clamp: the development of electrophysiology. Pflugers Arch. **453**(3), 233–247 (2006)
68. T. Tomita, A. Funaishi, Studies on intraretinal action potential with low-resistance microelectrode. J. Neurophysiol. **15**(1), 75–84 (1952)
69. G.S. Brindley, Responses to illumination recorded by microelectrodes from the frog's retina. J. Physiol. **134**(2), 360–384 (1956)
70. A.L. Byzov, Functional properties of different cells in the retina of cold-blooded vertebrates. Cold Spring Harb. Symp. Quant. Biol. **30**, 547–558 (1965)
71. S.R. Grabowski, L.H. Pinto, W.L. Pak, Adaptation in retinal rods of axolotl: intracellular recordings. Science **176**(4040), 1240–1243 (1972)
72. R.D. Penn, W.A. Hagins, Signal transmission along retinal rods and the origin of the electroretinographic a-wave. Nature **223**(5202), 201–204 (1969)
73. D.A. Baylor, T.D. Lamb, K.W. Yau, The membrane current of single rod outer segments. J. Physiol. **288**, 589–611 (1979)
74. D.A. Baylor, T.D. Lamb, K.W. Yau, Responses of retinal rods to single photons. J. Physiol. **288**, 613–634 (1979)
75. R.B. Barnes, M. Czerny, Läßt sich ein Schroteffekt der Photonen mit dem Auge beobachten? Zeitschrift für Physik **79**(7), 436–449 (1932)
76. S. Hecht, S. Shlaer, M.H. Pirenne, Energy, quanta, and vision. J. Gen. Physiol. **25**(6), 819–840 (1942)
77. E. Brumberg, S. Vavilov, Visuelle Messungen der statistischen Photonenschwankungen. Bull. Acad. Sci. U.R.S.S. **7**, 919–941 (1933)
78. E.M. Brumberg, S.I. Vavilov, Z.M. Sverdlov, Visual measurements of quantum fluctuations. I. The threshold of vision as compared with the results of fluctuation measurements. J. Phys. **7**(1), 1–8 (1943)
79. S.I. Vavilov, T.V. Timofeeva, Visual measurements of quantum fluctuations. II. Fluctuations when the eye is light-adapted. J. Phys. **7**(1), 9–11 (1943)
80. S.I. Vavilov, T.V. Timofeeva, Visual measurements of quantum fluctuations. III. The dependence of the visual fluctuations on the wave-length. J. Phys. **7**(1), 12–17 (1943)
81. S.I. Vavilov, *The Microstructure of Light* (Academy of Sciences, Moscow, 1950), p. 198. (in Russian)

82. S. Hecht, S. Shlaer, M.H. Pirenne, Energy at the threshold of vision. Science **93**(2425), 585–587 (1941)
83. R. Gunter, The absolute threshold for vision in the cat. J. Physiol. **114**(1–2), 8–15 (1951)
84. S. Hecht, M.H. Pirenne, The sensibility of the nocturnal long-eared owl in the spectrum. J. Gen. Physiol. **23**(6), 709–717 (1940)
85. M.C. Teich, P.R. Prucnal, G. Vannucci, M.E. Breton, W.J. McGill, Multiplication noise in the human visual system at threshold: 1. Quantum fluctuations and minimum detectable energy. J. Opt. Soc. Am. **72**, 419–431 (1982)
86. P.R. Prucnal, M.C. Teich, Multiplication noise in the human visual system at threshold: 2. Probit estimation of parameters. Biol. Cybern. **43**, 87–96 (1982)
87. M.C. Teich, P.R. Prucnal, G. Vannucci, M.E. Breton, W.J. McGill, Multiplication noise in the human visual system at threshold: 3. The role of non-poisson quantum fluctuations. Biol. Cybern. **44**, 157–165 (1982)
88. K.W. Yau, T.D. Lamb, D.A. Baylor, Light-induced fluctuations in membrane current of single toad rod outer segments. Nature **269**(5623), 78–80 (1977)
89. P.B. Detwiler, J.D. Conner, R.D. Bodoia, Gigaseal patch clamp recordings from outer segments of intact retinal rods. Nature **300**(5887), 59–61 (1982)
90. R.D. Bodoia, P.B. Detwiler, Patch-clamp recordings of the light-sensitive dark noise in retinal rods from the lizard and frog. J. Physiol. **367**, 183–216 (1985)
91. J. Toyoda, H. Hashimoto, H. Anno, T. Tomita, The rod response in the frog and studies by intracellular recording. Vis. Res. **10**(11), 1093–1100 (1970)
92. T. Tomita, Electrical activity of vertebrate photoreceptors. Q. Rev. Biophys. **3**(2), 179–222 (1970)
93. J.E. Brown, L.H. Pinto, Ionic mechanism for the photoreceptor potential of the retina of *Bufo marinus*. J. Physiol. **236**(3), 575–591 (1974)
94. R.R. Birge, R.B. Barlow, On the molecular origins of thermal noise in vertebrate and invertebrate photoreceptors. Biophys. Chem. **55**, 115–126 (1995)
95. N.M. Phan, M.F. Cheng, D.A. Bessarab, L.A. Krivitsky, Interaction of fixed number of photons with retinal rod cells. Phys. Rev. Lett. **112**, 213601 (2014)
96. L. Mandel, E. Wolf, *Optical Coherence and Quantum Optics* (Cambridge University Press, Cambridge, England, 1995)
97. F.T. Arecchi, Measurement of the statistical distribution of Gaussian and laser sources. Phys. Rev. Lett. **15**, 912 (1965)
98. D.N. Klyshko, *Physical Foundations of Quantum Electronics* (World Scientific, Singapore, 2011)
99. N. Sim, D. Bessarab, C.M. Jones, L. Krivitsky, Method of targeted delivery of laser beam to isolated retinal rods by fiber optics. Biomed. Opt. Express **2**, 2926–2933 (2011)
100. A.A. Malygin, A.N. Penin, A.V. Sergienko, Absolute calibration of the sensitivity of photodetectors using a biphotonic field. Sov. Phys. JETP Lett. **33**, 477–481 (1981)
101. H. Mutoh, W. Akemann, T. Knöpfel, Genetically engineered fluorescent voltage reporters. ACS Chem. Neurosci. **3**, 585–592 (2012)
102. K.D. Piatkevich, F.V. Subach, V.V. Verkhusha, Engineering of bacterial phytochromes for near-infrared imaging, sensing, and light-control in mammals. Chem. Soc. Rev. **42**(8), 3441–3452 (2013)
103. T. Tolmachova, O.E. Tolmachov, A.R. Barnard, S.R. de Silva, D.M. Lipinski, N.J. Walker, R.E. Maclaren, M.C. Seabra, Functional expression of Rab escort protein 1 following AAV2-mediated gene delivery in the retina of choroideremia mice and human cells ex vivo. J. Mol. Med. (Berl) **91**(7), 825–837 (2013)
104. E. Pomarico, B. Sanguinetti, N. Gisin, R. Thew, H. Zbinden, G. Schreiber, A. Thomas, W. Sohler, Waveguide-based OPO source of entangled photon pairs. New J. Phys. **11**, 113042 (2009)
105. V. Volkov, Discovering electrophysiology in photobiology: a brief overview of several photobiological processes with an emphasis on electrophysiology. Commun. Integr. Biol. **7**, e28423 (2014)